CONF-960202--18

LA-UR- 96- 684

Title: INFLUENCE OF THERMAL RESIDUAL STRESSES ON THE ELASTIC PHASE-STRAIN DEVELOPMENT IN METAL MATRIX COMPOSITES

Author(s): N. Shi, M. A. M. Bourke, J. A. Goldstone, J. E. Allison

Submitted to: proceedings of TMS meeting, Anaheim, CA 4-8 Feb 96

Los Alamos
NATIONAL LABORATORY

Form No. 836 R5
ST 2629 10/91

INFLUENCE OF THERMAL RESIDUAL STRESSES ON THE ELASTIC PHASE-STRAIN DEVELOPMENT IN METAL MATRIX COMPOSITES

N. Shi[1] M. A. M. Bourke[1] J. A. Goldstone[1], and J. E. Allison[2]

[1]Los Alamos National Laboratory
Los Alamos, NM 87545
[2]Scientific Research Laboratory, Ford Motor Company
Dearborn, MI 48121-2053

Abstract

The development of elastic lattice phase strains in a 15 vol. pct TiC particulate reinforced 2219-T6 Al composite was modeled as a function of tensile uniaxial loading by finite element method (FEM). In the relationship of applied stress vs. elastic lattice phase strain, the slopes vary with the applied load even before the macroscopic yielding. The slopes for the phase-strain perpendicular to loading follow nonmonotonic changes with loading, while, in the direction parallel to loading, the slopes change monotonically with the applied load. In this investigation, we have demonstrated via FEM that thermal residual stresses from thermal expansion mismatch between phases affect initiation of matrix plasticity. And the differences in the matrix plasticity initiation influence the internal stress distribution. The changes in the slope are dictated by the internal stress transfer between phases. FEM models with and without thermal history show significant differences in the response of elastic strain component, a mechanics equivalent of the lattice elastic strain. Agreement with experiment can only be obtained by including the thermal history. From a simple elasto-plastic spring model we are able to demonstrate that, with matrix plasticity propagating as predicted by FEM, the elastic strain component responds similarly to the more rigorous numerical predictions, suggesting that the morphology of elastic strain evolution is dictated by the development of matrix plasticity.

N. Shi, et al

Introduction

Thermal residual stresses (TRS) due to thermal mismatch between phases have been under investigation in a variety of composites for several years (e.g. [1-3]). TRS and related material microstructural changes have been found to influence the mechanical properties of metal matrix composites (MMCs) [4]. Recent investigations suggested that matrix plastic flow in MMCs is strongly influenced by the TRS [5-7], and that this influence is responsible for the observed asymmetric composite constitutive behavior between tension and compression [6-10]. However, many useful corollaries on the internal stress state were obtained numerically and have not been independently verified by experiment. One important experimental technique is diffraction, which provides phase-discriminative information on the state of average elastic strains. When conducted under load [11], *in situ* diffraction strain measurement probes into load transfer between phases, since elastic strain is proportional to the phase-stress.

In this investigation, the evolution of lattice phase-strains of a particle-reinforced Al/TiC composite under uniaxial tensile loading was studied. A numerical analysis was performed using the finite element method (FEM) to model the influence of TRS on the evolution of the lattice elastic phase-strains both parallel and perpendicular to the loading direction. The results were compared with the neutron diffraction measurements obtained using a compact stress rig at the Manuel Lujan Jr. Neutron Scattering Center (MLNSC) of Los Alamos National Laboratory. A simple spring-type model was developed to describe how the TRS affects the evolution of the lattice strains.

Experimental Background

The material used in this study was a 2219 Al alloy reinforced with 15 vol. pct TiC particles. The average diameter of the reinforcement was about 3 μm [12]. The composite was produced *in situ* by Martin Marietta using the XD™ process. The as-received composite was first extruded into plates, heat treated in T6 condition, then machined into a button-head cylindrical tensile specimen with a gauge length and diameter of 12.27 and 1.0 cm, respectively. The gauge length was arbitrarily selected for a free passage of the neutron beam without interference from the grips.

During diffraction measurements, lattice strains were measured as a function of applied uniaxial tensile load. A gauge length of 1.4 cm was illuminated by the neutron beam corresponding to a total irradiated volume of 1.1 cm^3. Initially, a tensile load of 200 MPa was applied, followed by unloading, to detect modifications of residual strain induced by a small load. Then, the specimen was loaded incrementally to 327 MPa sufficient to induce 1 pct total strain as recorded by a strain gauge attached to the specimen. The loading process was divided into intervals of approximately 50 MPa. Strains were measured at the end of each stress intervals. Average elastic lattice strain was obtained by Rietveld profile refinement of the entire diffraction spectrum [13].

Numerical Interpretation of Experimental Results

In this section, the results of three-dimensional (3-D) and two-dimensional (2-D) axisymmetric thermo-elasto-plastic FEM analyses are described. These results were compared with neutron diffraction data. To simplify the problem and obtain further understanding of the results, a simple averaging model developed to account for the numerical results is presented.

FEM Modeling

The composite was assumed to be an infinite cubic array of periodically distributed cubic particles embedded in the matrix with volume fraction of 15 pct. A full 3-D and a 2-D axisymmetric unit cell model with periodic boundary conditions was employed to study the development of average elastic phase strain and plastic strain distributions, respectively.

To understand the impact of TRS two different loading histories were examined. In the first case (History I), the composite was assumed to be stress-free at 200°C. A total temperature drop of

N. Shi, et al

180°C was uniformly applied in steps to all the nodal points in the mesh. After the cooling, a tensile uniaxial load was applied incrementally in a sequence: 0⇒200⇒0⇒327⇒0 MPa. To compare with a hypothetical composite devoid of the influence of TRS (designated as History II) cooling was not included before the same loading sequence.

Phenomenological Responses of the Average Lattice Strain. The FEM results under the History I are shown in Fig. 1 along with the diffraction profile refinement data. In Fig. 1 elastic lattice strain in each phase was plotted against the applied traction. In the direction parallel to the applied load as shown in Fig. 1(a) (in the remainder of the text, we refer this direction as the parallel direction; and likewise, the direction perpendicular to the loading as the perpendicular direction), the slope of the strain-traction curve for the matrix *increased* with the applied load even below the nominal composite yield stress (~ 320 MPa), while that for the corresponding particles *decreased*. Despite the differences in the sense of the slope changes, these changes were monotonic as shown in Fig. 1(a).

Along the perpendicular direction in Fig 1(b), the slope for the particle strain decreased initially with the load increase, and increased again at composite macro-yielding (above ~320 MPa). The slope for the matrix strain increased initially before a final decrease upon the composite macro-yielding, exhibiting "zigzag" slope changes. Based on the sense of slope changes, the development of elastic phase-strains can be characterized in three stages as shown in Fig. 1(b).

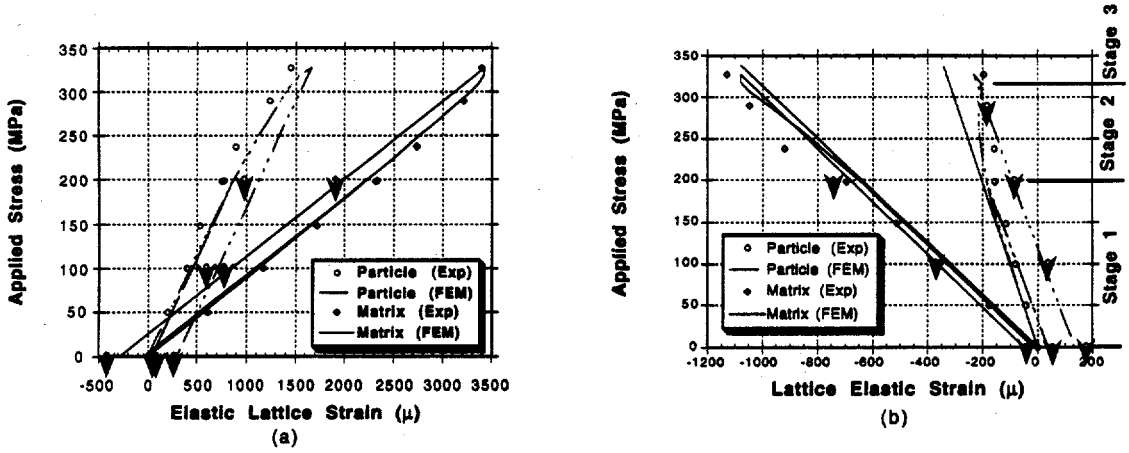

Figure 1: Comparisons of the evolution of the lattice phase-strains predicted by the FEM under the History I and the Rietveld profile refinement of the diffraction data, where data points with arrow (↓) are from unloading. (a) Parallel strains are shown. The changes of the slope are monotonic; (b) Perpendicular strains are shown. The changes of slope are nonmonotonic ("zigzag"). The straight lines are references to show the "zigzag." Three stages are defined based on the changes of slope.

Figure 2 displays the predicted increases of elastic lattice strains as a function of the applied stress under History II (no TRS). While the change of the slope was nonmonotonic (i.e., "zigzag" behavior) parallel to the loading direction [Fig. 2(a)], the slope of the lattice phase-strain evolution in the perpendicular direction in both phases changed monotonically [Fig. 2(b)].

Matrix Plastic Flow. Figure 3 shows the effective plastic strain contours ($\bar{\varepsilon}^p = \sqrt{\frac{2}{3}\varepsilon_{ij}^p \varepsilon_{ij}^p}$) in the matrix predicted by the axisymmetric model under the prescribed History I (with TRS). Four applied stress levels were selected (i.e., 0, 160, 270 and 327 MPa); the nonzero stress values were selected within each of the three characteristic stages specified in Fig. 1(b).

As the applied load increased to 160 MPa [Fig. 3(a)], the effective plastic strain developed between the two adjacent particles perpendicular to loading direction near the particle-matrix interface. Plasticity appeared in the matrix at 270 MPa between two particles aligned parallel to

N. Shi, et al
3
10

loading [upper-left corner of the unit cell in Fig. 3(b)]. When the applied load reached 327 MPa as shown in Fig. 3(c), the two matrix regions with plastic flow interconnected.

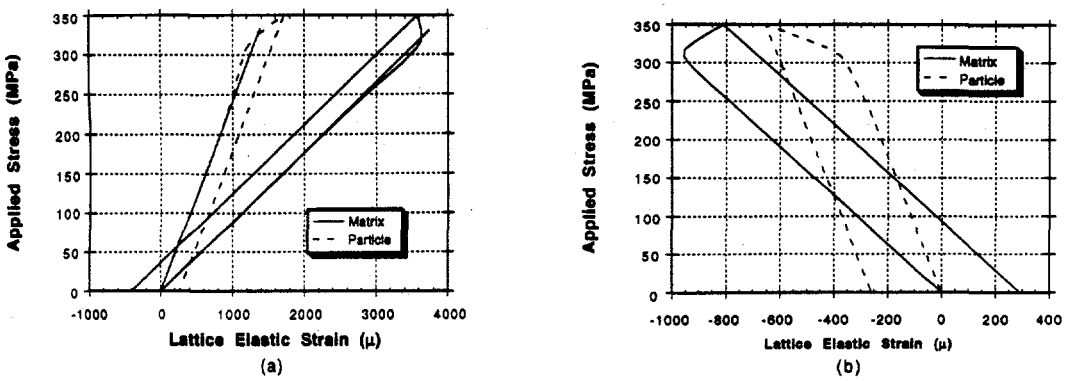

Figure 2: Lattice phase-strains predicted by the FEM following the History II where the thermal history is not considered. (a) Parallel strains are shown. The changes of slope are nonmonotonic ("zigzag"). This behavior is the same as that expected from diffusion-controlled stress relaxation [11]. The straight lines are references to show the "zigzag." (b) Perpendicular strains are shown. The changes of slope are monotonic.

Figure 4 displays the distributions of the matrix effective plastic strain under History II (no TRS) at 270 and 327 Mpa (at 160 MPa no matrix plasticity was developed). At 270 MPa [Fig. 4(a)], in contrast with the History I, plasticity appeared between particles aligned in the parallel direction, and spread to the rest of matrix at higher loads [e.g., at 327 MPa in Fig. 4(b)].

From Figs. 3 and 4, it is evident that the initial TRS determines the location of the plastic flow initiation. In the three stages characterized by the slopes in Fig. 1(b), the evolution of matrix plastic flow goes through three different stages: (1) elastic matrix; (2) plastic flow initiation; and (3) continuous plastic matrix. In the next section, we will investigate the influence on the response of the average lattice phase-strains by the shift of the plastic flow initiation site.

An Elasto-Plastic Spring Model

With the assumption that material becomes a viscous continuum when plastically deforming, elastic strain (and therefore stresses) cannot further develop in the flow region in a non-hardening material. This necessitates stress redistribution in the composite when far-field load continues to increase. To model this phenomenon, a three-component 2-D unit cell (*ABCD*)was constructed as shown in Fig. 5, each with two springs oriented perpendicular and parallel to loading, providing stiffness in these directions. The matrix components were simplified as elasto-plastic springs, with tangential moduli K ($K = E^{(m)}$, the matrix young's modulus; and after yielding $K = E_h$, the work hardening rate), while the particle remains elastic. The cell boundary remains straight and the springs are connected either in series or in parallel accordingly as dictated by the arrangement shown in Fig. 5. As an example to show the zigzag behavior, we simulate the development of internal perpendicular elastic strains in the unit cell in different stages as indicated in the previous section, and follow the sequence of plastic initiation accordingly.

The perpendicular internal stresses are caused by the differential Poisson's contractions from different components under the applied stress, $\Delta\sigma^A$:

$$\Delta\varepsilon_{11}^{(1)} = -\frac{\nu^{(1)}\Delta\sigma^A}{K^{(1)}}; \tag{1}$$

$$\Delta\varepsilon_{11}^{(2,3)} = -\frac{\nu^{(r)}}{E^{(r)}}\Delta\sigma_{22}^{(r)}\sqrt{f} - \frac{\nu^{(2)}}{K^{(2)}}\Delta\sigma_{22}^{(2)}\left(1-\sqrt{f}\right), \tag{2}$$

N. Shi, et al 4/10

PEMAG

	VALUE
1	+5.00E-10
2	+5.00E-04
3	+1.00E-03
4	+1.50E-03
5	+2.00E-03
6	+2.50E-03
7	+3.00E-03
8	+3.50E-03
9	+4.00E-03
10	+4.50E-03
11	+5.00E-03

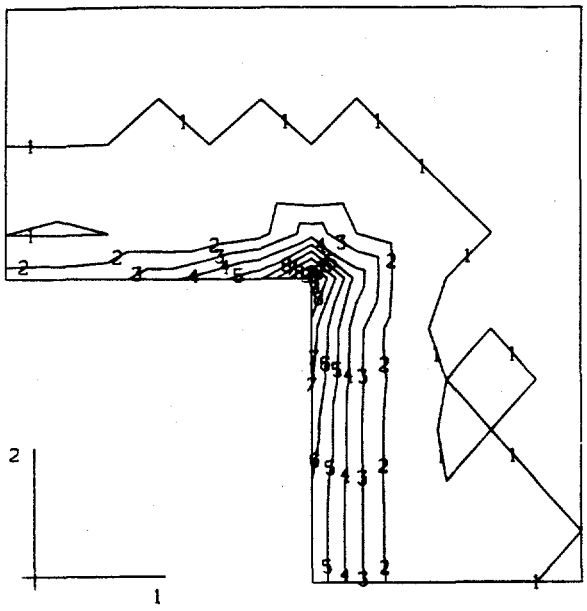

(a)

PEMAG

	VALUE
1	+5.00E-10
2	+5.00E-04
3	+1.00E-03
4	+1.50E-03
5	+2.00E-03
6	+2.50E-03
7	+3.00E-03
8	+3.50E-03
9	+4.00E-03
10	+4.50E-03
11	+5.00E-03

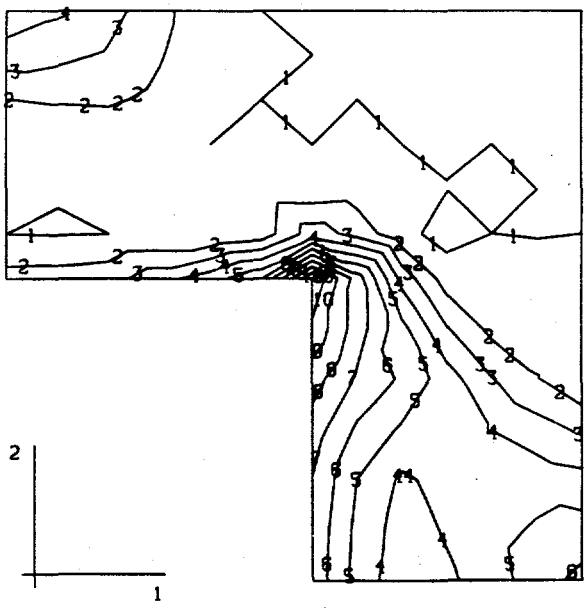

(b)
(overleaf)

N Shi, et al

5

10

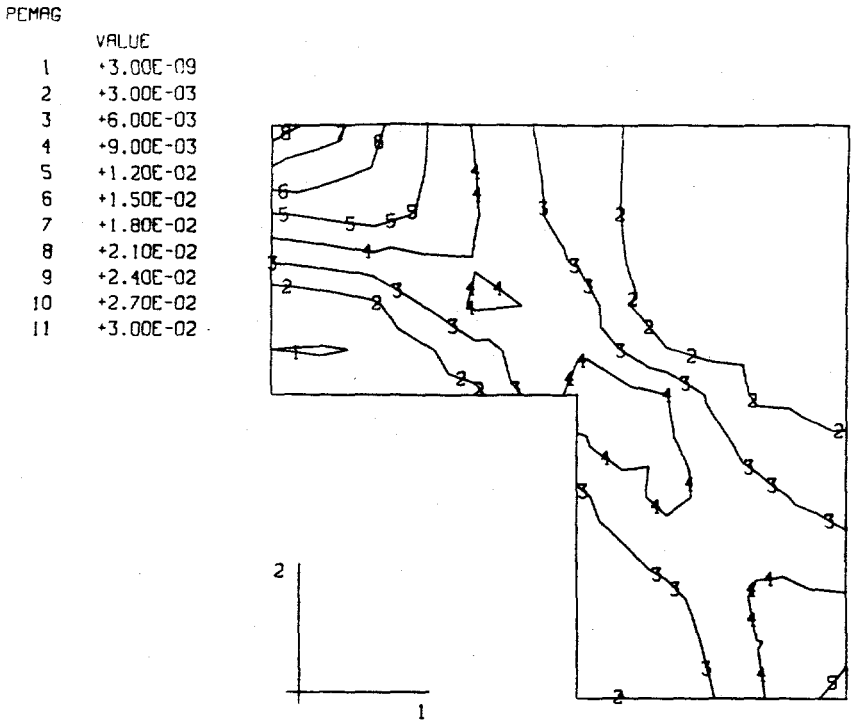

(c)

Figure 3: Matrix-effective plastic strain contours under the History I when the applied stress is (a) 160 MPa; (b) 270 MPa; and (c) 327 MPa. Matrix plastic flow first developed near parallel interface and propagated to matrix above the particle.

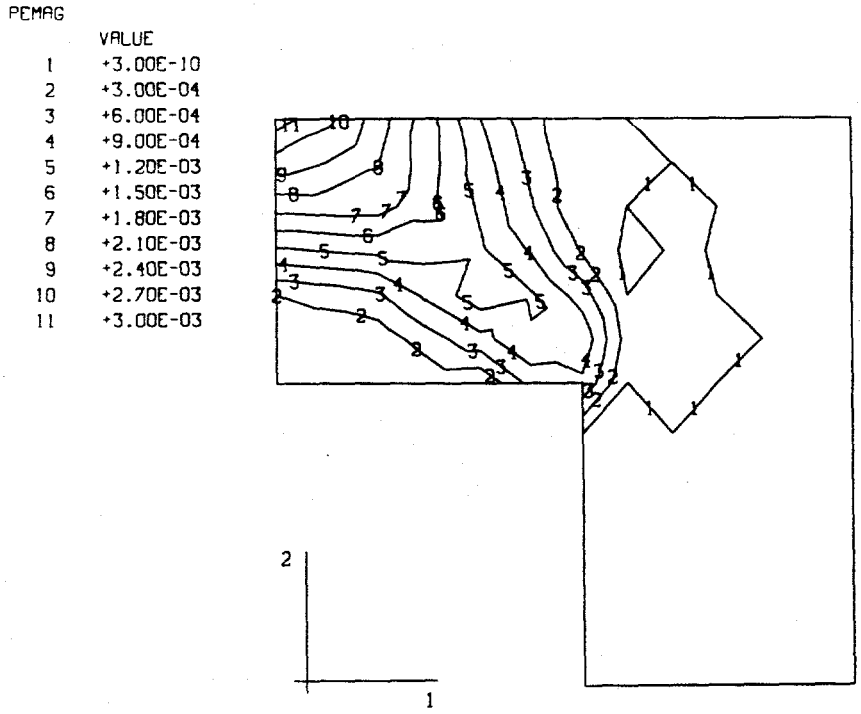

(a)
(overleaf)

N. Shi, et al

6

10

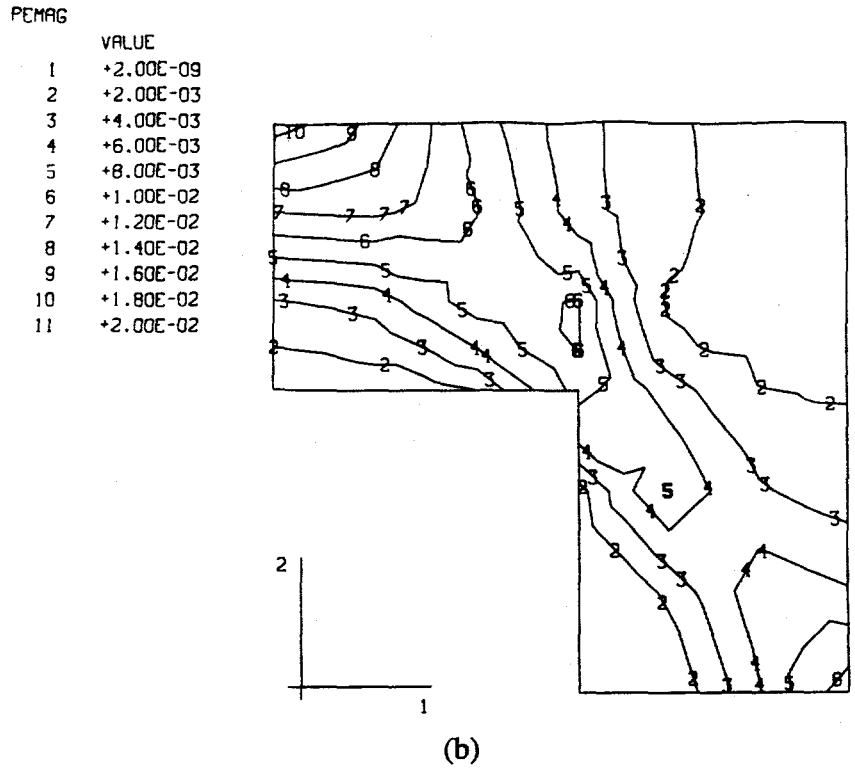

(b)

Figure 4: Matrix-effective plastic strain contours under the History II when the applied stress is (a) 270 MPa; (b) 327 MPa. Matrix plastic flow first developed above the particle and propagated to the side of the particle. At or below 160 MPa, no matrix plasticity was developed.

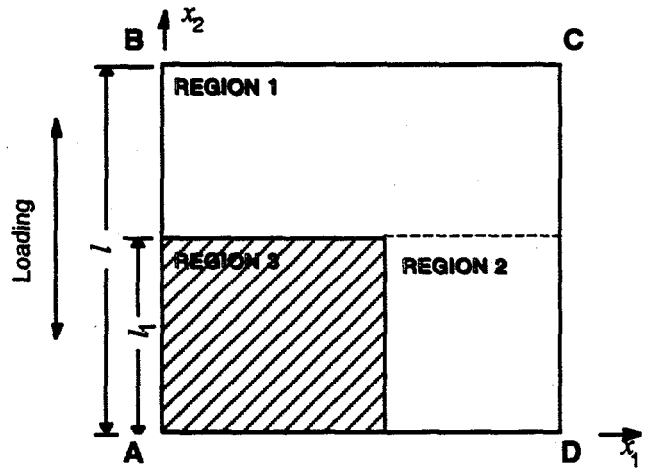

Figure 5: Partitions of the unit cell into different components for the spring model. The shaded area is the particle.

where $f=\left(l_1/l\right)^2$ is the reinforcement volume fraction. The $\Delta\varepsilon_{11}^{(1)}$ and $\Delta\varepsilon_{11}^{(2,3)}$ are the strain increment in region 1 and the total strain increment from regions 2 and 3 connected in series, respectively. $E^{(r)}$ represents the Young's modulus of the reinforcement. The $\nu^{(i)}$ is the Poisson's ratio, where the superscripts (1), (2), and (3) [or (r)] stand for the regions 1, 2, and 3 [or the reinforcement]. The superscripts (i,j), where i,j=1, 2, or 3, denote average collective response from the regions i and j when they are considered as *one* combined domain.

The regions 2 and 3 may be approximated to follow isostrain condition when deforming along x_2, and we obtain:

$$\Delta\sigma^A=\sqrt{f}\Delta\sigma_{22}^{(r)}+\left(1-\sqrt{f}\right)\Delta\sigma_{22}^{(2)}; \tag{3}$$

$$\frac{\Delta\sigma_{22}^{(r)}}{E^{(r)}}=\frac{\Delta\sigma_{22}^{(2)}}{K^{(2)}}. \tag{4}$$

By considering, along the parallel boundary $\overline{CD}$, the conditions of equilibrium and inter-cell compatibility, the following equations may be obtained:

$$\Delta\sigma_{11}^{(1)}\sqrt{f}+\Delta\sigma_{11}^{(2,3)}\left(1-\sqrt{f}\right)=0 \tag{5}$$

$$\Delta\varepsilon_{11}^{(1)}+\frac{\Delta\sigma_{11}^{(1)}}{K^{(1)}}=\Delta\varepsilon_{11}^{(2,3)}+\left(\frac{1-\sqrt{f}}{K^{(2)}}+\frac{\sqrt{f}}{E^{(r)}}\right)\Delta\sigma_{11}^{(2,3)}. \tag{6}$$

By solving Eqs. 1 to 6, the increments of four stresses and the two strains can be obtained. The changes of elastic strain component in each region, $\Delta e_{11}^{(i)}$, can then be expressed as a function of that of the stresses from the Hooke's law. With an area-average of these strain increments, the average increment of matrix elastic strain component, $\left\langle\Delta e_{11}^{(m)}\right\rangle$, is given by

$$\begin{aligned}\left\langle\Delta e_{11}^{(m)}\right\rangle&=\frac{1}{1+\sqrt{f}}\left(\Delta e_{11}^{(1)}+\sqrt{f}\Delta e_{11}^{(2)}\right)\\&=\frac{1}{E^{(m)}\left(1+\sqrt{f}\right)}\left\{\Delta\sigma_{11}^{(1)}+\sqrt{f}\Delta\sigma_{11}^{(2,3)}-\nu^{(m)}\left[\frac{K^{(2)}\sqrt{f}\Delta\sigma^A}{K^{(2)}+\left(E^{(r)}-K^{(2)}\right)\sqrt{f}}\right]\right\},\end{aligned} \tag{7}$$

where

$$\Delta\sigma_{11}^{(1)}=\frac{\Delta\varepsilon_{11}^{(2,3)}-\Delta\varepsilon_{11}^{(1)}}{\frac{1}{K^{(1)}}+\frac{\sqrt{f}}{K^{(2)}}+\frac{f}{1-\sqrt{f}}\frac{1}{E^{(r)}}}, \tag{8}$$

and $\Delta\sigma_{11}^{(2,3)}$ may be obtained from Eq. 5.

By substituting into Eq. 7 the spring constants according to the predicted pattern of plastic flow propagation at different stages, the slope changes under TRS can be obtained. Table 1 shows the slopes ($s=\Delta\sigma^A/\left\langle\Delta e_{11}^{(m)}\right\rangle$) and the corresponding materials constants. The slopes follow the order of $|s_3|>|s_1|>|s_2|$, consistent with the FEM results [Fig. 1(b)].

Table 1: Change of slope predicted by Eq. 7

Loading stage	Region 1	Region 2	$s = \frac{\Delta\sigma^A}{\langle \Delta e_{11}^{(m)} \rangle}$ ($\times 10^5$ MPa)
Stage 1	$K^{(1)} = E^{(m)}$; $\nu^{(1)}$=0.3 (Elastic)	$K^{(2)} = E^{(m)}$; $\nu^{(2)}$=0.3 (Elastic)	-4.5
Stage 2	$K^{(1)} = E^{(m)}$; $\nu^{(1)}$=0.3 (Elastic)	$K^{(2)} = E_h^{(m)}$; $\nu^{(2)}$=0.5 (Plastic)	-3.4
Stage 3	$K^{(1)} = E_h^{(m)}$; $\nu^{(1)}$=0.5 (Plastic)	$K^{(2)} = E_h^{(m)}$; $\nu^{(2)}$=0.5 (Plastic)	-36

In this analysis, many assumptions are made to make the model simple. However, by correctly representing the pattern of the matrix plastic flow and that the matrix tangential stiffness, K, decreases at the place where plastic flow starts (elasto-plastic spring), the analysis predicts the same trends as those from both diffraction and FEM.

Discussion

In this investigation, we have achieved good agreement between FEM modeling and the profile refinement of the neutron diffraction measurements. FEM analysis indicated that the plastic-flow initiation site in the matrix is altered by the inclusion of TRS. When considered this influence, a simple spring model can predict the "zigzag" lattice strain increases in the perpendicular direction. The changes of slope at a relatively low load level imply that changes of load-sharing between the two phases occur before macro yielding and that the initial load-sharing is affected by the TRS.

It is also interesting to note that the results from this investigation reveal some significant differences with a previous work. In a particulate-reinforced Al/SiC composite, Allen et al. [11] observed that the slope changes of the lattice phase-strains under applied loading were nonmonotonic in both parallel and perpendicular directions. Withers suggested that diffusion-controlled stress relaxation during loading led to this phenomenological response. Based on their modeling, they argued that TRS had no influence on the lattice phase-strain response. However, with little evidence of creep stress relaxation during our measurements, both diffraction and FEM results (with TRS) (Fig. 1) show that, while similar *nonmonotonic* slope changes are observed for lattice phase-strain along the perpendicular direction, the changes of slope are *monotonic* parallel to the load (Fig. 1). On the other hand, the relaxation-controlled response in the parallel direction [11] has a similar morphology with that when TRS is not considered [Fig. 2(a)].

To have an insight into the correlation between the two mechanisms (i.e., diffusion vs. TRS), we need to compare their influences on the matrix deformation. For diffusion stress relaxation, as the sample is pulled, the atoms diffuse from the side to the top of the particle. This type of stress relaxation is partially promoted by a large gradient of matrix dilatational stress, which is more tensile at the top of the particle. From the perspective of unrecoverable deformation, the diffusion flux along the interfaces leads to permanent contraction along the "side" in the *perpendicular* direction, which is equivalent to plastic flow between the two perpendicular adjacent particles [Fig. 1(b)]; diffusion also induces permanent matrix elongation between particles aligned in the parallel direction, which is equivalent to plastic flow initiation without the influence of TRS [Fig. 2(a)]. Therefore, the strain response under diffusion stress relaxation shares similarities with that affected by TRS in the *perpendicular* direction, and that without TRS in the *parallel* direction. FEM can capture the effects of TRS because it accounts for localized flow, which is overlooked by the mean field approach.

Conclusions

The following conclusions can be drawn from this investigation:

(1) Good agreement has been achieved between FEM modeling and the average phase-strain obtained from neutron diffraction during *in situ* loading. Slope changes in the load-induced lattice strain response are nonmonotonic in the perpendicular direction, and monotonic in the parallel direction.

(2) FEM results indicate that the aforementioned lattice phase-strain response can best be predicted by considering the effects of TRS. TRS helps plastic flow in the matrix between perpendicular-aligned particles. Without TRS, matrix plastic flow initiates between parallel-aligned particles in the particle array.

(3) Results from the elasto-plastic spring model show that this unique morphology of plastic flow initiation induced by TRS is responsible for the observed response of matrix lattice strain.

Acknowledgments

Manuel Lujan Jr. Neutron Scattering Center is a national user facility funded by the United States Department of Energy, Office of Basic Energy Science. This work was supported in part by DOE contract W7405-ENG-36.

Reference

[1] H. M. Ledbetter and M. W. Austin: Mater. Sci. Eng., 1987, vol. 89, pp. 53-61.
[2] S. Majumdar, J. P. Singh, D. S. Kupperman, and A. D. Krawitz: Eng. Mater. Tech., 1991, vol. 113 51-59.
[3] M. A. M. Bourke, J. A. Goldstone, and T. M. Holden: in Measurement of Residual and Applied Stress Using Neutron Diffraction, M. T. Hutchings and A. D. Krawitz, eds., Kluwer Acd. Pub., Netherland, 1992, pp. 369-82.
[4] N. Shi and R. J. Arsenault: Ann. Rev. Mater. Sci., 1994, vol. 24, pp. 321-57.
[5] N. Shi, B. Wilner, and R. J. Arsenault: Acta Metall. Mater., 1992, vol. 40, pp. 2841-54.
[6] L. C. Davis and J. E. Allison: Metall. Trans A., 1993, vol. 24A, pp. 2487-96.
[7] A. Levy and J. M. Papazian: Acta Metall. Mater., 1991, vol. 39, pp. 2255-66.
[8] P. J. Withers, W. M. Stobbs, and O. B. Pedersen: Acta Metall., 1989, vol. 37, pp. 3061-84.
[9] T. Nakamuru and S. Suresh: Acta Metall. Mater., 1993, vol. 41, pp. 1665-81.
[10] N. Shi and R. J. Arsenault: Scripta Metall. Mater., 1993, vol. 27, pp. 623-8.
[11] A. J. Allen, M. A. M. Bourke, S. Dawes, M. T. Hutchings, and P. J. Withers: Acta Metall. Mater., 1992, vol. 40, pp. 2361-73.
[12] G. M. Vyletel, D. C. Van Aken, and J. E. Allison: Scripta Metall. Mater., 1991, vol. 25, pp. 2405-10.
[13] R. B. Von Dreele, J. D. Jorgenen, and C. G. Windsor: J. Appl. Crystallogr., 1982, vol. 15, pp. 581-9.

N. Shi et al.

10

10